Combustion and Flame 157 (2010) 363–373

Contents lists available at ScienceDirect

Combustion and Flame

journal homepage: www.elsevier.com/locate/combustflame

Bio-butanol: Combustion properties and detailed chemical kinetic model

G. Black, H.J. Curran, S. Pichon, J.M. Simmie *, V. Zhukov

Combustion Chemistry Centre, National University of Ireland, Galway, Ireland

ARTICLE INFO

Article history:
Received 30 April 2009
Received in revised form 9 June 2009
Accepted 6 July 2009
Available online 3 August 2009

Keywords:
Bio-butanol
Modelling
Ignition delay
Bond dissociation energy
Butan-1-ol

ABSTRACT

Autoignition delay time measurements were performed at equivalence ratios of 0.5, 1 and 2 for butan-1-ol at reflected shock pressures of 1, 2.6 and 8 atm at temperatures from 1100 to 1800 K. High-level ab initio calculations were used to determine enthalpies of formation and consequently bond dissociation energies for each bond in the alcohol. A detailed chemical kinetic model consisting of 1399 reactions involving 234 species was constructed and tested against the delay times and also against recent jet-stirred reactor speciation data with encouraging results. The importance of enol chemistry is highlighted.

1. Introduction

The current usage of fossil fuels must be curbed because of global warming brought about by the exhaust products of combustion and because it is simply unsustainable [1]. In the medium to long term, biofuels—here, liquid or gaseous fuels produced from biomass and primarily destined for use in the transport sector—are expected to make a significant contribution to reduce our dependence on fossil fuels [2]. However, it is not yet clear which biofuels will emerge as the best possible choices for spark-ignition and compression-ignition engines nor indeed for gas turbines.

Bio-ethanol is at present the most widely produced biofuel and is used both as an additive to petrol/gasoline and as a fuel in its own right in specially-modified vehicles. Recent work suggests that it may worsen local air quality and hence have a deleterious impact on human health [3]. It also suffers from a number of drawbacks, including low energy density, high vapour pressure and high solubility in water, as well as compounding the problem of ground water contamination due to MTBE leakage from underground storage tanks [4].

Other alcohols can be produced from biomass either directly or via gasification and further processing. In particular, bio-butanol (*n*-butanol or butan-1-ol) has emerged [5] as a possible candidate for consideration partly because it does not suffer from the same drawbacks as ethanol. Indeed butanol is known to increase water uptake in a hydrocarbon fuel and thereby boost the octane rating and decrease emissions of NO_x [6]. In a direct comparison of 10% blends in gasoline, Wallner et al. [7] have found that butanol performs equally as well as ethanol in a direct-injection spark-ignition engine from a standpoint of regulated emissions and combustion, but with the advantage of decreased fuel consumption. In addition, a new method of production [8] which does not involve the classical fermentation route is promising, as are new developments in the critical area of separation [9].

There is little previous work on the pyrolysis and oxidation of butanol in the literature. Barnard [10] measured the rate of pyrolysis of butan-1-ol between 846 and 902 K at sub-atmospheric pressure and determined a rate constant of $1.58 \times 10^{12} \exp(-28,500/T)\ s^{-1}$ with an activation energy of 237 kJ mol^{-1}. More recently McEnally and Pfefferle [11] carried out a comparative study of each of the four isomers of butanol in a co-flowing methane/air flame. They identified two principal decomposition pathways, four-centred elimination producing H_2O and a butene, and C–C bond fission, followed by β-scission of the resulting radicals to produce alkenes, aldehydes and ketones. The latter process was found to be dominant for butan-1-ol. Interestingly they found that in comparison to butane the butanols generated much larger concentrations of aldehydes and ketones, suggesting that the exhaust emissions of toxic by-products might be a bigger issue with oxygenated biofuels.

Yang et al. [12] investigated low pressure laminar premixed butanol flames using synchrotron radiation photoionisation and molecular beam mass spectrometry to identify transient and stable species. Their results, although not quantitative, are extremely valuable from the viewpoint of mechanism construction.

Dagaut and Togbé [13] have studied the oxidation kinetics of a butanol–surrogate gasoline 85:15 blend in a jet-stirred reactor at

* Corresponding author.
E-mail address: john.simmie@nuigalway.ie (J.M. Simmie).
URL: http://c3.nuigalway.ie/ (J.M. Simmie).

0010-2180/$ - see front matter © 2009 The Combustion Institute. Published by Elsevier Inc. All rights reserved.
doi:10.1016/j.combustflame.2009.07.007

10 atm and from 770 to 1220 K with initial fuel concentrations of 0.1 mol%. Their final kinetic mechanism of 251 species and 1990 reversible reactions summarizes the reactions of the butanol, iso-octane, toluene and 1-hexene mixture.

Dagaut and co-workers [14] studied the oxidation of pure butan-1-ol in a jet-stirred reactor at 10 atm and over a range of equivalence ratios. High-levels of carbon monoxide, carbon dioxide, water, hydrogen, methane, formaldehyde, ethylene, and propene were detected and the results used to validate a detailed chemical kinetic mechanism.

These authors have very recently published an updated version of their model, along with the new experimental data against which it is tested, consisting of species profiles in an opposed-flow diffusion flame and at atmospheric pressure in a jet-stirred reactor, as well as laminar flame speeds [15].

Moss and colleagues [16] have measured the autoignition of all four isomers of butanol behind reflected shock waves and carried out kinetic modelling showing that H-atom abstraction from the most reactive isomers, 1- and iso-butanol, is primarily responsible for fuel consumption.

As part of a long-running programme of investigations into the combustion chemistry of oxygenates [17–33] and in conjunction with new high-level computational studies of the dehydration reactions [34] and H-atom abstraction reactions [35] by $\dot{O}H$ and $H\dot{O}_2$ from *n*-butanol, and, of the formation of enols from hydroxyalkyl radicals [36] we have carried out autoignition delay measurements behind reflected shock waves over a range of equivalence ratios, pressures and temperatures and assembled a detailed chemical model to account for these and other recent experiments.

2. Experimental

The butan-1-ol (anhydrous, 99.8% pure) was supplied by Sigma–Aldrich and de-gassed through a series of freeze–thaw–pump cycles, after which no more gas was observed to escape on thawing the solid. The oxygen (99.5% pure) and argon (99.9% pure) were supplied by BOC. Mixtures were made up using the method of partial pressures and their compositions are given in Table 1.

Bio-butanol experiments have been performed at equivalence ratios of 0.5, 1 and 2 and at a range of pressures 1–8 atm over a range of temperatures from 1100 to 1800 K. The main part of the data was obtained at a dilution level of ~95%, but one series was measured at a dilution of 77% with argon as the diluent in all experiments. The range of possible conditions under which to study the gas-phase oxidation of butanol was limited by its low vapour pressure under ambient conditions, which is 10 mbar at 28 °C. Mixtures were therefore made up with butanol partial pressures well below the saturation vapour pressure.

The incident shock velocity at the endwall was used to calculate the temperature and pressure of the mixture behind the reflected shock wave using the equilibrium program Gaseq [37]. The thermodynamic data for butan-1-ol was calculated using the THERM program of Ritter and Bozzelli [38], based on group additivity methods developed by Benson [39]. These data are in agreement with estimates in the NIST WebBook [40] and with the Burcat and Ruscic database [41].

Table 1
Butanol mixture compositions; balance argon. p_5 = reflected shock pressure.

p_5/atm	Φ	% Butan-1-ol	% O_2
1.0	2.0	0.75	2.25
1.0	1.0	0.75	4.5
1.0	0.5	0.75	9.0
2.6	1.0	0.6	3.6
2.6	1.0	3.5	21.0
8.0	2.0	0.6	1.8
8.0	1.0	0.6	3.6
8.0	0.5	0.6	7.2

2.1. High pressure shock tube

The stainless steel shock tube has an overall length of 8.76 m, with an internal diameter of 63 mm. A double-diaphragm section divides the shock tube into a 3 m long driver section and a 5.73 m test section. Polycarbonate films were used as diaphragms in all experiments, and shock waves were fired by the self-rupture of diaphragms. The operational pressure limit of the shock tube is approximately 60 bar.

The diagnostic system involves four pressure transducers and one photomultiplier. The speed of the incident shock wave is measured at three locations and is then extrapolated to the end-plate. Typical attenuation of the shock wave amounts to 2–4% over a distance of 1 m. The shock tube has two optical windows, one in the end-plate and one in the side-wall at a distance of 7 mm from the end-plate.

Ignition delay times can be determined from time histories of the pressure and/or light emission. For these experiments we defined them as the time between arrival of the shock wave at the end-plate and the 50% level of the first strong peak of the light signal from the end-plate. Prior to the butanol experiments the tube was tested with experiments on *n*-heptane ignition; our data is in good agreement with experiments from the Hanson group [42].

2.2. Low pressure shock tube

The low pressure shock tube consists of a test section measuring 6.22 m in length, with an internal diameter of 10.24 cm, and a barrel-shaped driver section measuring 53 cm in length. The two sections were separated by a polycarbonate diaphragm, which burst when forced into contact with a cross-shaped cutter due to the pressure differential between the high pressure driver section and the low pressure test section. The driver gas used was helium (99.99% pure; BOC).

Four pressure transducers located along the last half metre of the tube were used to determine the velocity of the incident shock wave. The velocity at the endwall was determined through linear extrapolation, so as to take attenuation of the shock wave into account.

The pressure at the endwall was monitored by a pressure transducer (Kistler, model 603B). Light emission at 431 nm was detected through a fused silica window embedded in the end-plate using a photodetector (Thorlabs Inc. PDA55-EC) and a narrow band-pass filter centred at 430 nm with a full-width half-maximum of 10 nm. The ignition delay time was defined as the interval between the rise in pressure due to the arrival of the shock wave at the endwall and the maximum rate of rise of the emission signal. The shock tube was validated before and after performing this work by comparison of ignition delay values for *n*-heptane mixtures to those obtained previously [42,43].

2.3. Thermochemistry

The bond dissociation energies (BDEs), D(X–Y), of butan-1-ol are not well-known [44] so a number of computations were performed to determine these. We have used the CBS-QB3 methodology [45,46] as implemented in Gaussian-03 [47] together with isodesmic [48] and, in some cases, isogeitonic [49] reactions to compute the enthalpy of formation at 298.15 K of the appropriate radical and hence D(C–H), Table 2, and D(O–H), Table 3. We have assumed a 10% error in the computed enthalpy of reaction and expressed the resultant error at the 95% confidence level. Here we

Table 2
Formation enthalpies, ΔH_f(298.15 K), and bond dissociation energies (**this work**).

Ṙ	$\Delta H_f(\dot{R})$/kJ mol^{-1}		D(C—H)/kJ mol^{-1}	
$CH_3CH_2CH_2\dot{C}HOH$	**−95.5 ± 2.7**		**397 ± 3**	397.2 [44]
$CH_3CH_2\dot{C}HCH_2OH$	**−74.0 ± 2.8**		**419 ± 3**	
$CH_3\dot{C}HCH_2CH_2OH$	**−79.6 ± 2.2**		**413 ± 2**	
$\dot{C}H_2CH_2CH_2CH_2OH$	**−68.7 ± 1.8**		**424 ± 2**	
$CH_3CH_2\dot{C}HOH$	**−75.4 ± 2.9**	−81 ± 4 [64]	**398 ± 3**	392–400 [44]
$CH_3\dot{C}HCH_2OH$	**−59.8 ± 2.6**	−78.7 ± 8.4 [57]	**413 ± 3**	394.6 ± 8.4 [57]
$\dot{C}H_2CH_2CH_2OH$	**−48.6 ± 1.8**	−66.9 ± 8.4 [44]	**425 ± 2**	406.3 ± 8.4 [44]
$CH_3\dot{C}HOH$	**−57.2 ± 2.7**	−55.6 ± 3.3 [65], −54.0 [44]	**396 ± 3**	389–401 [44]
$\dot{C}H_2CH_2OH$	**−26.0 ± 1.6**	−29.3[66], −31 ± 7 [67]	**427 ± 2**	410–424 [44]

Table 3
Formation enthalpies, ΔH_f(298.15 K), and bond dissociation energies (**this work**).

Ṙ	$\Delta H_f(R\dot{O})$/kJ mol^{-1}		D(O—H)/kJ mol^{-1}	
Me	—	+21.0 ± 2.1 [62]	—	440.0 ± 2.2 [62]
Et	**−12.3 ± 1.5**	−13.6 ± 4.0 [62]	**441 ± 2**	439.2 ± 4.0 [62]
nPr	**−33.4 ± 1.7**	−30.1 ± 8.4 [68]	**440 ± 2**	432.6 ± 4.2 [69], 443.1 ± 8.4 [68]
nBu	**−53.9 ± 2.1**	−62.8 [69]	**439 ± 2**	426.3 ± 4.2 [69]

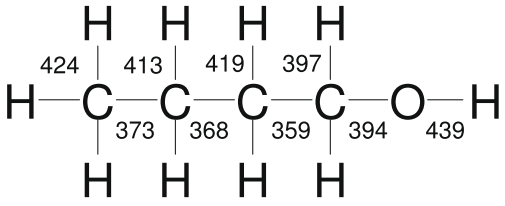

Fig. 1. Bond dissociation energies of butan-1-ol/kJ mol^{-1}.

have chosen the lowest energy TGt conformer of butanol [50] on which to base our computations.

Our computed C–H bond dissociation energies are independent of the heat of formation of butan-1-ol, which ranges from −275 to −280 kJ mol^{-1} [51–54] with -275.0 ± 0.4 kJ mol^{-1} preferred [55], but the radical formation enthalpies are directly linked. The calculated values are in satisfactory agreement with comparable C_α—H bond energies in the lower normal alcohols; for example, Luo [44] recommends 401.2 ± 4.2 for ethanol, quoting a range of values from 392 to 400 kJ mol^{-1} for *n*-propanol and just 397 kJ mol^{-1} for butanol. Our results of 396 ± 3, 398 ± 3 and 397 ± 3 kJ mol^{-1}, respectively, suggest that these bonds have effectively the same strength.

The terminal H—$CH_2\cdots$OH bond energies for ethanol, propanol and butanol that we compute of 427 ± 2, 425 ± 2 and 424 ± 2 are in good agreement with the 422 ± 8 kJ mol^{-1} for ethanol [44], but not with the 410 ± 8 of Ruscic et al. [56], nor with the 406 ± 8 for *n*-propanol [57].

The only slight surprise is that the $CH_3\dot{C}HCH_2CH_2OH$ radical is more stable than $CH_3CH_2\dot{C}HCH_2OH$ by some 6 kJ mol^{-1}, which in turn affects their respective C–H BDEs. However, both higher level calculations, CBS-APNO [58], and group additivity predictions [39] support this inequality, which probably stems from the hyperconjugative stabilising effect of the terminal methyl group. Overall the computed C–H BDEs are approximately in accord with predictions, based on structure–activity relationships developed for reactions of atmospheric interest, for the important channels in the reaction of $\dot{O}H$ with butan-1-ol by Yujing and Mellouki [59]:

$$CH_3CH_2CH_2CH_2OH + \dot{O}H \xrightarrow{58\%} CH_3CH_2CH_2\dot{C}HOH + H_2O$$

$$CH_3CH_2CH_2CH_2OH + \dot{O}H \xrightarrow{20\%} CH_3CH_2\dot{C}HCH_2OH + H_2O$$

$$CH_3CH_2CH_2CH_2OH + \dot{O}H \xrightarrow{17\%} CH_3\dot{C}HCH_2CH_2OH + H_2O$$

Abstraction from the terminal methyl or the OH groups is much less important. A more recent estimate [60] suggests that the probabilities of attack by $\dot{O}H$ at the O, α, β, γ and δ hydrogens are as follows: 2.2:42.7:38.3:14.7:2.2.

Theoretical calculations at the BH&HLYP/6-311G(d,p) level, improved by single-point computations at CCSD(T) with the same basis set, by Galano et al. [61] indicate that abstraction of the γ-H predominates over that from α or β hydrogens but only below 350 K. Extrapolation to temperatures of interest here gives abstraction rates of α:β:γ = 9.1:0.7:1.0.

In the case of the alkoxy radicals we have chosen to base our computations on the most recent critical evaluation [62] for $CH_3\dot{O}$ which yielded $\Delta H_f(298.15\ K) = 21.0 \pm 2.1$ kJ mol^{-1}, equivalent to D(O–H) of 440.0 ± 2.2 kJ mol^{-1}, to determine firstly $CH_3CH_2\dot{O}$, then $CH_3CH_2CH_2\dot{O}$ and finally $CH_3CH_2CH_2CH_2\dot{O}$ (these are at variance with recent work by Tumanov and Denisov [63] who have derived values that are consistently lower by some 8 kJ mol^{-1}). The resulting D(O–H) values that we calculate, Table 3, are not inconsistent with the premise that lengthening the hydrocarbon chain has little effect on the O–H bond strength [70].

The C–C and C–OH energies were calculated from our values in Tables 2 and 3 together with $\Delta H_f(\dot{C}H_2OH) = -17.0 \pm 0.7$ and $\Delta H_f(\dot{O}H) = 37.3 \pm 0.3$ kJ mol^{-1} from Ruscic et al. [62] to give a complete picture of bond energies for butanol, Fig. 1.

The C–OH energy of 390 ± 2 kJ mol^{-1} is in satisfactory agreement with values derived by Luo [44] from data of Pedley et al. [55] for ethanol of 393 ± 3, propanol of 394 ± 3 and butan-1-ol of 392 ± 4 kJ mol^{-1}. The C–C energies follow the same trend as those computed via a PM3 formalism by Hatipoğlu and Çinar [71], but are substantially higher by 50—90 kJ mol^{-1}. Our value of 359 for the C_α—C_β bond strength is in good agreement with the 357.3 ± 3.3 kJ mol^{-1} quoted by Luo [44] and the terminal C_γ—C_δ bond strength of 373 agrees well with the corresponding bond in *n*-butane of 372 kJ mol^{-1} [44].

3. Model

The mechanism is based on our updated C_4 chemistry [72], with a butanol sub-mechanism added that was loosely taken from one generated using the EXGAS program [73] and then modified as appropriate.

3.1. Unimolecular decomposition

The butanol sub-mechanism includes the two possible classes of unimolecular decomposition reaction – simple and complex fission. According to our calculations, the weakest bond in the molecule is the C_α—C_β bond, as would be expected given its proximity to the electron withdrawing hydroxyl group. This is consistent with the

experimental findings of Barnard [10], who proposes fission of this bond to be the primary decomposition pathway on the basis that formaldehyde is the predominant pyrolysis product observed, while other aldehydes and lower alcohols are absent. The remaining bond dissociation energies follow the order shown in Fig. 1 and this is reflected in the fission rates, with breaking of the C–O bond not competitive.

All of the simple fission decomposition reactions were treated as bimolecular:

$$CH_3CH_2CH_2CH_2OH + M \overset{1320}{\rightarrow} \dot{C}H_3 + \dot{C}H_2CH_2CH_2OH + M$$

$$CH_3CH_2CH_2CH_2OH + M \overset{1321}{\rightarrow} CH_3\dot{C}H_2 + \dot{C}H_2CH_2OH + M$$

$$CH_3CH_2CH_2CH_2OH + M \overset{1322}{\rightarrow} CH_3CH_2\dot{C}H_2 + \dot{C}H_2OH + M$$

$$CH_3CH_2CH_2CH_2OH + M \overset{1323}{\rightarrow} CH_3CH_2CH_2\dot{C}H_2 + \dot{O}H + M$$

$$CH_3CH_2CH_2CH_2OH + M \overset{1324}{\rightarrow} CH_3CH_2CH_2CH_2\dot{O} + \dot{H} + M$$

The high-pressure limit rate constants for each of these reactions were calculated from microscopic reversibility using an estimate of the rate constant for radical–radical recombination. For reaction (−1320) a rate constant of $1.373 \times 10^{13} \exp(472.7/T)$ $cm^3\ mol^{-1}\ s^{-1}$ was used similar to that recommended by Tsang [74] for methyl recombination with *tert*-butyl radical. For reactions (−1321) and (−1322) a rate constant of 2.0×10^{13} $cm^3\ mol^{-1}\ s^{-1}$ was used which is that recommended by Tsang [75] for the recombination of ethyl and *n*-propyl radicals to form *n*-pentane.

Reaction (−1323) was estimated to be 2.41×10^{13} $cm^3\ mol^{-1}\ s^{-1}$ as recommended by Tsang [74] for the recombination of hydroxyl radical with *tert*-butyl radical. Finally, the rate constant for reaction −1324 was estimated to be 1.0×10^{14} $cm^3\ mol^{-1}\ s^{-1}$ which we commonly use for hydrogen atom addition to other free radicals.

A chemical activation formulation based on Quantum Rice–Ramsperger–Kassel theory, as described by Dean [76,77] was then used together with the high-pressure limit expressions to develop pressure-dependent rate constants which were ultimately fit to a nine-parameter Troe formalism [78].

Complex fission may take place through a number of different pathways, but the only one considered here is the four-centred elimination of water, forming 1-butene:

$$CH_3CH_2CH_2CH_2OH + M \overset{1325}{\rightarrow} CH_3CH_2CH{=}CH_2 + H_2O + M$$

Calculations show that the barrier heights for the other three dehydration pathways are too large for them to be competitive [35].

McEnally and Pfefferle [11], in their study of the four isomers of butanol, found that the importance of this pathway depended on the extent of branching in the structure. They report this to be the predominant decomposition pathway for *t*-butanol, but to be of little importance in the case of the straight chain butan-1-ol. As they did nonetheless find small amounts of butene in their flames and as this species was also detected by Yang et al. [12], we included this pathway in our mechanism. However, it is important to note that 1-butene can also be formed by decomposition of the β radical:

$$CH_3CH_2\dot{C}HCH_2OH \overset{1335}{\rightarrow} CH_3CH_2CH{=}CH_2 + OH$$

The rate constant expression for the elimination reaction was determined using our calculated barrier height of 281 kJ mol^{-1} [35] and an A-factor estimated based on Tsang's work [79] on the elimination of water from alkyl-substituted butanols.

3.2. Hydrogen abstraction

Rate constants for hydrogen abstraction from the γ and δ positions were taken as identical to those previously published for abstraction from 1° to 2° carbons in alkanes [80]. As the bond dissociation energy of the hydrogen at the β position was found to be intermediate between that of the γ and δ hydrogens, the rate of abstraction was calculated as the average of the two. Abstractions at the α position and from the hydroxyl group were likened to the equivalent reactions of ethanol [81–83] where possible. As the hydrogen of the alcohol group is both the most tightly bound and statistically the least likely to be abstracted, this pathway is not expected to be important, as observed by previous authors [11]. For abstraction from the α position by $\dot{O}H$:

$$CH_3CH_2CH_2CH_2OH + \dot{O}H \overset{1353}{\rightarrow} CH_3CH_2CH_2\dot{C}HOH + H_2O$$

using the rate constant of Dagaut et al. [14] gave better agreement with calculated bond dissociation energies and this value was therefore adopted.

3.3. Isomerisation

Isomerisation of the first-formed radicals is potentially an important determinant of reactivity and also of the type of by-products formed, as they decompose to form different oxygenated and non-oxygenated compounds depending on the location of the radical site. Isomerisation reactions were included only where they proceed via 4- or 5-centred transition states, on the grounds that 3-centred hydrogen transfer is energetically too demanding to be of significance. The reactions considered are as follows therefore:

$$CH_3CH_2CH_2\dot{C}H_2 \overset{715}{\rightarrow} CH_3\dot{C}HCH_2CH_3$$

$$CH_3CH_2CH_2\dot{C}HOH \overset{1385}{\rightarrow} CH_3\dot{C}HCH_2CH_2OH$$

$$CH_3CH_2CH_2\dot{C}HOH \overset{1386}{\rightarrow} \dot{C}H_2CH_2CH_2CH_2OH$$

$$CH_3CH_2\dot{C}HCH_2OH \overset{1387}{\rightarrow} \dot{C}H_2CH_2CH_2CH_2OH$$

3.4. Radical decomposition

The first-formed radicals decompose primarily by β-scission, but it was also necessary to include reactions with molecular oxygen in order to improve our simulated jet-stirred reactor species profiles.

$$\dot{C}H_2CH_2CH_2CH_2OHx \overset{1387}{\rightarrow} CH_2{=}CH_2 + \dot{C}H_2CH_2OH$$

$$CH_3\dot{C}HCH_2CH_2OH \overset{1389}{\rightarrow} CH_3CH{=}CH_2 + \dot{C}H_2OH$$

$$CH_3\dot{C}HCH_2CH_2OH \overset{1390}{\rightarrow} CH_2{=}CHCH_2CH_2OH + \dot{H}$$

$$CH_3\dot{C}HCH_2CH_2OH \overset{1391}{\rightarrow} CH_3CH{=}CHCH_2OH + \dot{H}$$

$$CH_3CH_2\dot{C}HCH_2OH \overset{1392}{\rightarrow} CH_2{=}CHCH_2OH + \dot{C}H_3$$

$$CH_3CH_2\dot{C}HCH_2OH \overset{1393}{\rightarrow} CH_2{=}CHCH_2CH_3 + \dot{O}H$$

$$CH_3CH_2\dot{C}HCH_2OH \overset{1394}{\rightarrow} CH_3CH{=}CHCH_2OH + \dot{H}$$

$$CH_3CH_2CH_2\dot{C}HOH \overset{1395}{\rightarrow} CH_2{=}CHOH + \dot{C}_2H_5$$

$$CH_3CH_2CH_2\dot{C}HOH \overset{1396}{\rightarrow} nCH_3CH_2CH_2CHO + \dot{H}$$

$$CH_3CH_2CH_2\dot{C}HOH \overset{1397}{\rightarrow} CH_3CH_2CH{=}CHOH + \dot{H}$$

It is interesting to note that the decomposition of these radicals results in the formation of a number of different unsaturated alcohols—ethenol ($CH_2{=}CHOH$), 2-propen-1-ol ($CH_2{=}CHCH_2OH$), 1-buten-1-ol ($CH_3CH_2CH{=}CHOH$), 2-buten-1-ol ($CH_3CH{=}CHCH_2OH$) and 3-buten-1-ol ($CH_2{=}CHCH_2CH_2OH$). Of these, the true enols—ethenol and 1-buten-1-ol—are capable of tautomerising to form the corresponding aldehydes, Fig. 2. However, in the gas phase these enolic species will be produced and so reactions involving their formation and consumption must be included together with their thermochemistry.

Fig. 2. Keto/enol tautomerism of 1-buten-1-ol.

All rate constants for these reactions were estimated based on the work of Curran [85]; alkyl radical β-scission reactions are endothermic processes, thus this type/class of reaction is considered in the reverse, exothermic direction, the addition of a smaller alkyl/alkoxy radical to an olefin with the rate constant for the decomposition of the parent radical calculated using microscopic reversibility. Reactions −1388, −1389, −1392 and −1395 were considered to be similar to a methyl or an ethyl radical addition to ethylene or propene/ethenol with a rate constant of $8.80 \times 10^3 T^{2.48} \exp(-3085/T)$ cm^3 mol^{-1} s^{-1} for ethyl addition to propene/ethenol or propyl addition to ethylene. For methyl addition to propene a frequency factor of 1.76×10^4 cm^3 mol^{-1} s^{-1} is recommended, which is twice that for methyl addition to propene. Reaction −1395 also involves the addition of an ethyl radical to a C–C which is bonded to an OH group and we have used the same activation energy barrier for addition to propene and ethenol. This is justified as ab-initio quantum chemistry calculations [36] have yielded identical activation energy barriers for addition to the terminal carbon atom in both propene ($H_2C{=}CHCH_3$) and ethenol ($H_2C{=}CHOH$).

Reactions −1390, −1391, −1394, −1396, and −1397 all involve the generation of a C4 enol with the elimination of a hydrogen atom. Rate constants for the reverse addition of a hydrogen atom to the olefin are taken to be identical to those for hydrogen atom addition to ethylene and propene as provided in [85]. Finally, a rate constant of $9.93 \times 10^{11} \exp(483/T)$ cm^3 mol^{-1} s^{-1} was estimated for the addition of an hydroxyl radical to 1-butene (reaction −1393), with the rate constant for the decomposition of $CH_3CH_2\dot{C}HCH_2OH$ calculated via microscopic reversibility.

The carbonyl form is thermodynamically favoured—in the case of butenol to butanal isomerisation by −36 kJ mol^{-1} [84]—so that in solution, where acid/base catalysis is possible, such molecules exist predominantly in the keto form. In the gas phase however, conversion from the enol to the keto form cannot be easily catalysed, and it is therefore possible for the enol form to persist—the barrier height for isomerisation is ≈243 kJ mol^{-1} [84]. Commonly used methods of species detection, such as gas chromatography or mass spectrometry, are not isomer specific and the two forms cannot therefore be distinguished. However, recent developments in the field of molecular beam mass spectrometry using synchrotron radiation to selectively photo-ionise species has changed this picture completely and it is now possible to identify isomers unambiguously [86]. By exploiting this method, Yang and co-workers [12] have identified ethenol, propenol and butenol in their butan-1-ol flames, although quantitative results have yet to be published. Although there is a lack of kinetic data for these species, the three isomers of buten-1-ol have been included in our mechanism.

The final mechanism, nBuOHv1.0, consists of 1399 reactions involving 234 species and is freely available at http://c3.nuigalway.ie.

4. Comparison to experiment

Simulations were performed with different versions of the application Chemkin including Chemkin-Pro [87], using the Closed Homogeneous Batch Reactor model at constant volume for our shock tube experiments and the Perfectly Stirred Reactor model for the jet-stirred reactor experiments of Dagaut and co-workers [14].

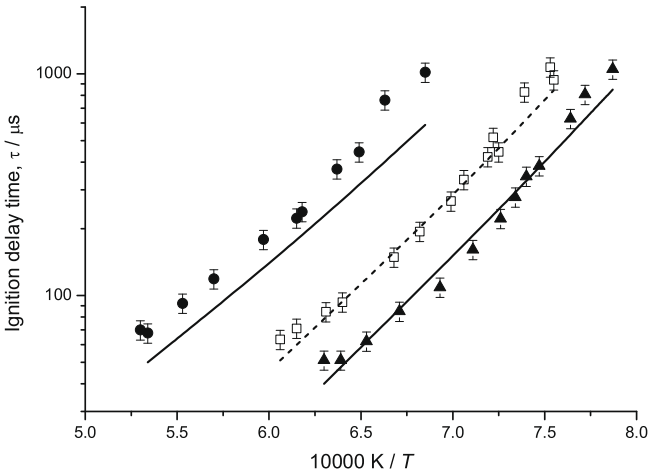

Fig. 3. Ignition delay times for 0.75% butan-1-ol in argon at 1 atm, ▲ 9% O_2 $\Phi = 0.5$, □ 4.5% O_2 $\Phi = 1.0$, ● 2.25% O_2 $\Phi = 2.0$, lines simulation.

4.1. Ignition delays

At 1 atm, the effect of increasing the oxygen concentration from 2.25% ($\Phi = 2.0$), to 4.5% ($\Phi = 1.0$), to 9.0% ($\Phi = 0.5$) is depicted in Fig. 3. Here we observe the high negative dependence of ignition time on oxygen which is observed at high temperatures ($1100 \leqslant T \leqslant 2000$ K) for almost all hydrocarbon and oxygenated hydrocarbon fuels. The predicted ignition delays agree well with measured values for lean and stoichiometric conditions, but at $\Phi = 2$ the simulation is too fast across the temperature range. However, the model does capture the dependence on increasing oxygen concentration quite well in that the higher the concentration of oxygen the faster is the ignition. So as to assess whether the disparity under rich conditions was due to radical recombination reactions delaying ignition, we tested the effect of adding C_5 chemistry to our model, but no change resulted. Thus, it would seem that this disparity is due to the current underlying mechanism. We have noted in the past [88] that hydrogen atom abstraction reactions from the fuel are more important to overall reactivity at lean conditions and that unimolecular fuel decomposition reactions are more important at rich conditions. Thus, the ratio of unimolecular decomposition to hydrogen atom abstractions may not be quite right.

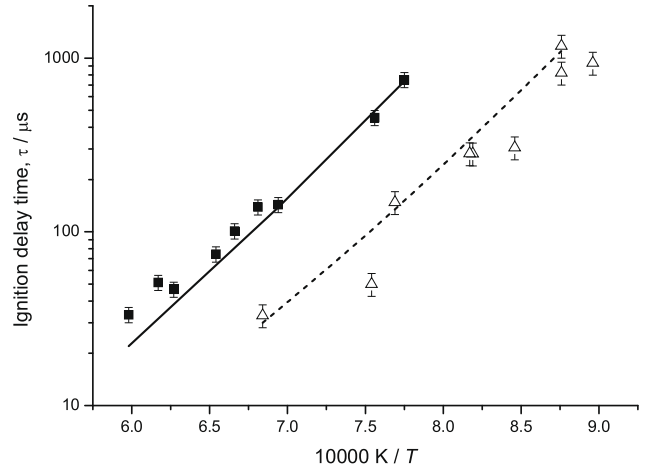

Fig. 4. Ignition delay times in argon at 2.6 atm, ■ 0.6% butan-1-ol, 3.6% O_2 $\Phi = 1.0$, △ 3.5% butan-1-ol, 21% O_2 $\Phi = 1.0$, lines simulation.

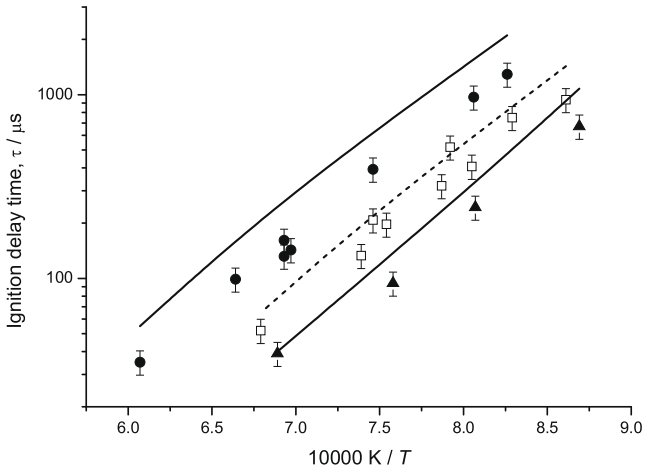

Fig. 5. Ignition delay times for 0.6% butan-1-ol in argon at 8 atm, ▲ 7.2% O_2 $\Phi = 0.5$, □ 3.6% O_2 $\Phi = 1.0$, ● 1.8% O_2 $\Phi = 2.0$, — simulation.

At 2.6 atm, the agreement is good for both dilute and concentrated stoichiometric mixtures, Fig. 4, and at 8 atm, the model performs reasonably well for $\Phi = 1$ and 0.5, although becoming too slow at lower temperatures for this latter, Fig. 5. The principal disparity is again observed for rich mixtures, although in this case the model over-predicts the delay time.

It is interesting to note that in Figs. 3 and 4 at pressures of 1.0 and 2.6 atm, respectively, the slope is concave down, but at 8.0 atm, the slope is concave up. At 1.0 and 2.6 atm the temperature range is such that high temperature kinetics dominate. However, at 8 atm, the lower temperatures of 1100 K are beginning to encapsulate the intermediate temperature regime where hydroperoxyl radical chemistry is more important.

4.2. Species profiles

Major and minor species profiles were simulated for mixtures of 0.1% butanol with oxygen and nitrogen at $\Phi = 0.5$, 1 and 2, at 10 atm and $\tau = 0.7$ s [14]. Results for lean conditions are shown in Fig. 6, for stoichiometric in Fig. 7 and for rich in Fig. 8. For all three mixtures, the model captures the behaviour of most species reasonably well, although the simulated butanol profile shows the fuel to be disappearing too fast. The greatest disagreement is observed in the case of ethyne, which the model over-predicts, and also for butanal, which is underpredicted.

Reactions of the first-formed radicals with molecular oxygen were not initially included in the mechanism, but were incorporated in order to improve the simulated butanal profiles. This did increase the amount of the aldehyde being formed according to the model, but not to the level found experimentally. The formation of butanal directly from the fuel via elimination of H_2 was considered, but preliminary calculations at the CBS-APNO level indicate a barrier height of 359 kJ mol^{-1} for this reaction, implying that it is unlikely to be competitive with the other unimolecular decomposition pathways – compare for example, the 281 kJ mol^{-1} barrier for the four-centred elimination of water.

Finally, we considered the possibility that some of the fuel radical β-scission reactions 1388–1397, described above, are responsible for forming C4 butenol species (1390, 1391, 1394, 1397). In fact our model predicts that much larger quantities

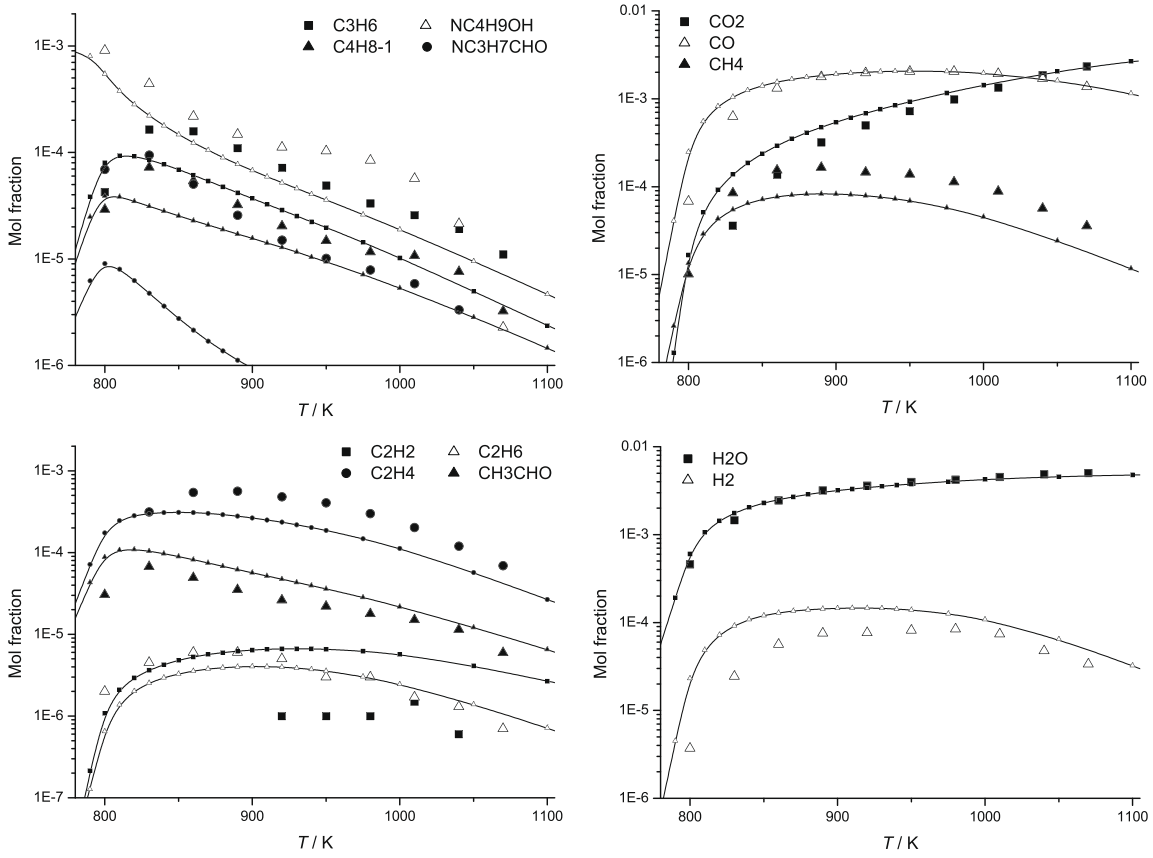

Fig. 6. Species profiles for 0.1% butan-1-ol, $\Phi = 0.5$, 10 atm, $\tau = 0.7$ s , lines simulation.

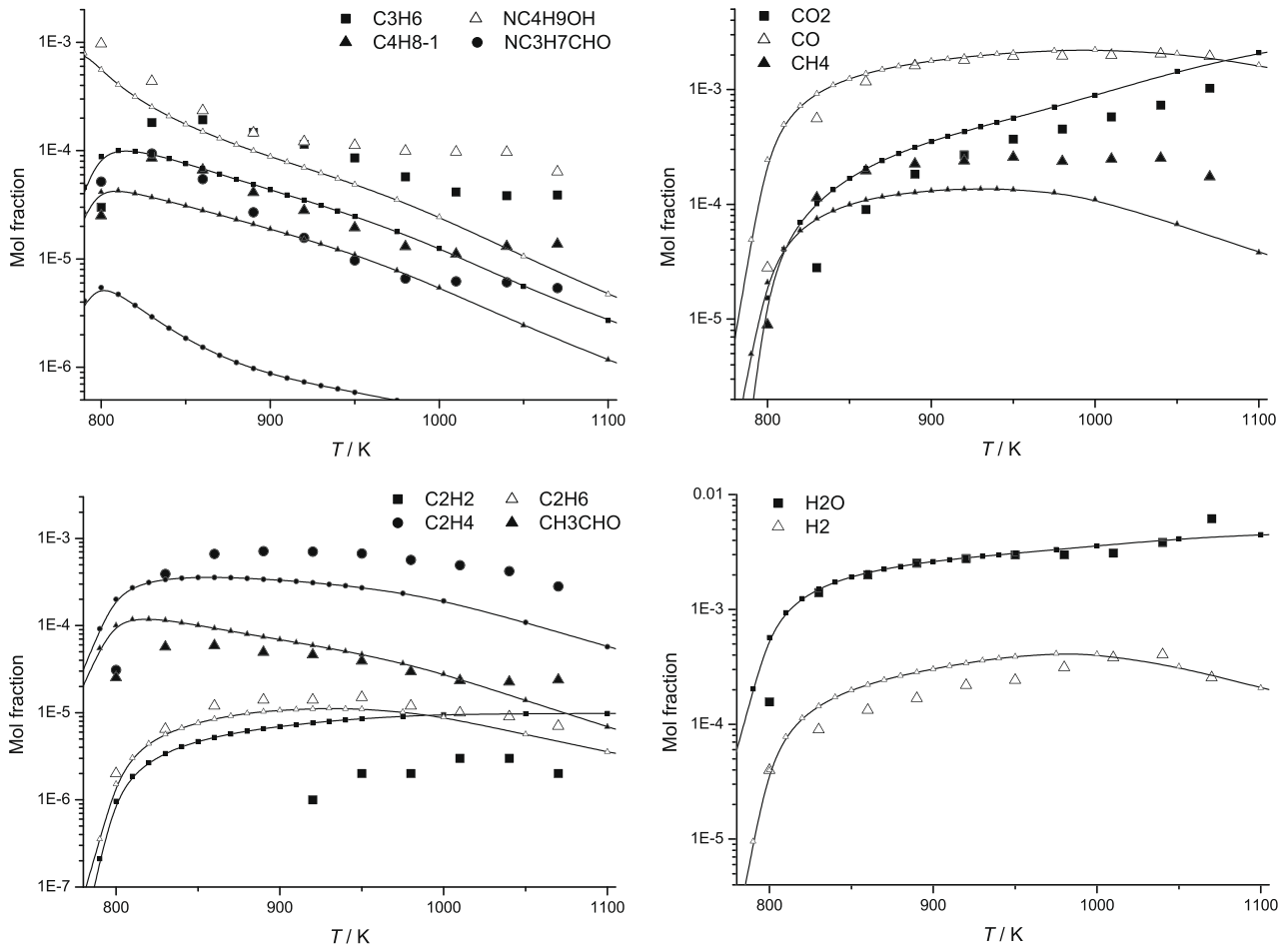

Fig. 7. Species profiles for 0.1% butan-1-ol, $\Phi = 1.0$, 10 atm, $\tau = 0.7$ s , lines simulation.

of buten-1-ol will be formed relative to butanal, see Fig. 9 for the $\Phi = 2$ mixture—similar considerations apply for the other two mixtures at $\Phi = 0.5$ and $\Phi = 1$. Since buten-1-ol will almost certainly tautomerise rapidly once it exits the reactor and before it is detected by the analytical system the reported "butan-1-al" concentrations are we believe more properly described as the sum of butanal + buten-1-ol. Note that the agreement is now considerably improved between experiment (points) and the simulation (solid line), Fig. 9.

We found a similar situation with acetaldehyde, Figs. 10 and 11. The model-predicted profile of ethanal or acetaldehyde (CH_3CHO) is almost an order of magnitude *lower* than that measured experimentally. However, the profile for ethenol (CH_2═CHOH) is very similar to that measured experimentally for "acetaldehyde" in the lean, stoichiometric and rich mixtures. It is highly probable that rapid tautomerisation of ethenol to ethanal is also occurring somewhere between the reactor exit and the analytical system.

4.3. Reaction path and sensitivity analysis

A reaction path analysis was carried out for the shock tube conditions outlined in Fig. 12, which shows H-abstraction to be the principal route of consumption of butanol, in accordance with modelling results reported in the literature [16,14]. Abstraction from the α position dominates, followed by the γ, β and δ positions, while abstraction from the hydroxyl group is of much lesser importance. By comparison, unimolecular decomposition accounts for only 25% of butanol consumption. Although McEnally and Pfefferle [11] report simple fission to be the dominant decomposition pathway for butanol, this is for non-premixed flames, where the concentration of small radicals capable of hydrogen abstraction is relatively low.

In order to ascertain which reactions are important for the shock tube data at $\Phi = 2$, where the model performs poorly, a sensitivity analysis was carried out at 1450 K and at pressures of 1, 2.6 and 8 atm. The 16 most sensitive reactions are shown in Figs. 13–15. The usual small radical reactions were found to have the greatest influence on ignition delay time, while the most sensitive fuel reaction at all three pressures is scission of the C_α—C_β bond, which has the effect of increasing the overall reactivity of the system. Abstraction from the β position by Ḣ atom and elimination of water also feature at all three pressures, but delay ignition. Abstraction from the β position by ȮH radical appears at 8 atm only, but it is apparent that formation of the β radical, which leads primarily to the production of but-1-ene, ultimately decreases the reactivity of the system.

5. Conclusions

Ignition delay times, measured using two different shock tubes, have been presented for butan-1-ol over a range of equivalence

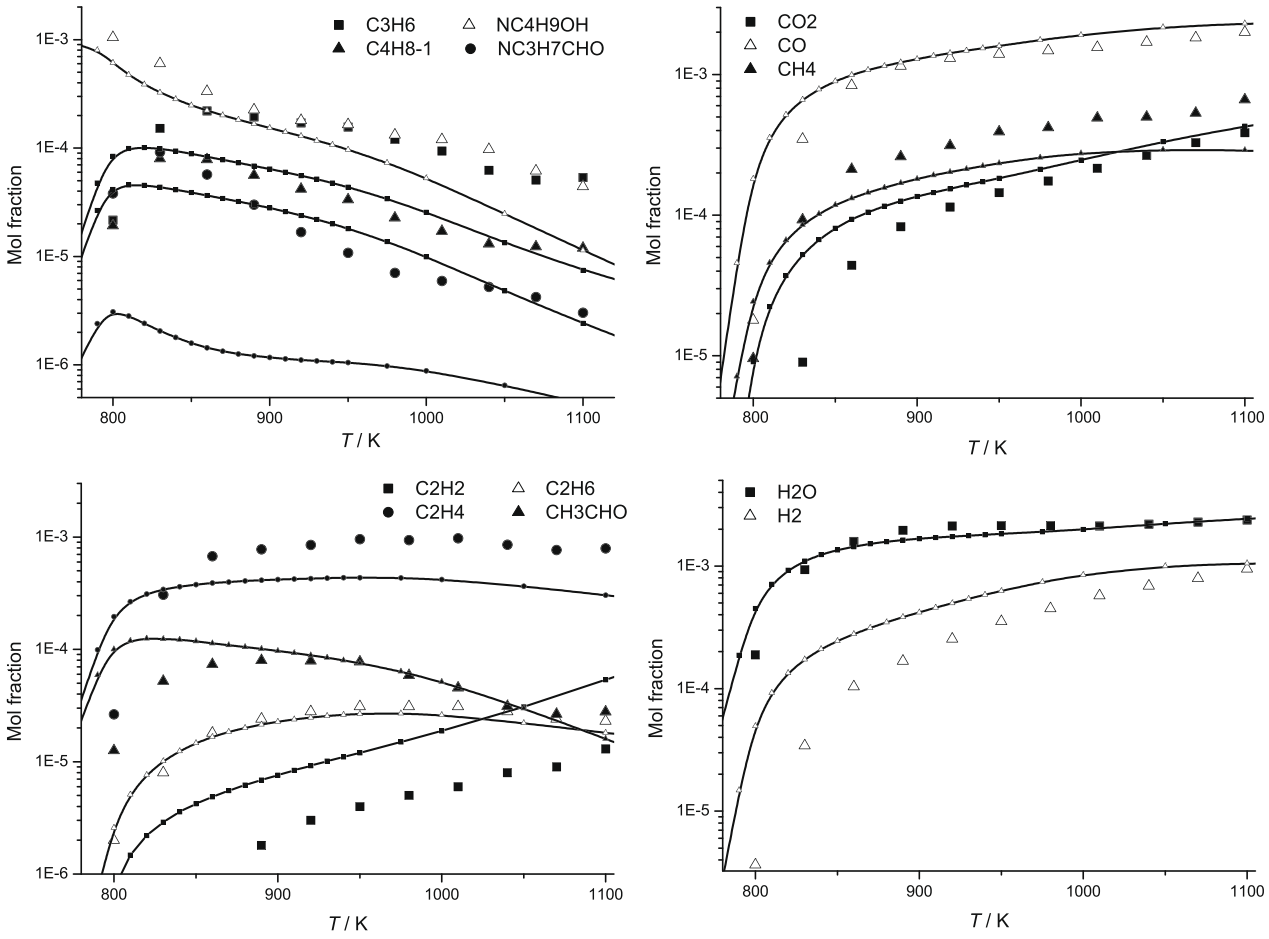

Fig. 8. Species profiles for 0.1% butan-1-ol, $\Phi = 2.0$, 10 atm, $\tau = 0.7$ s, lines simulation.

ratio, pressures of 1–10 atm and in the temperature range 1100–1800 K. The results of thermochemical calculations at the CBS-QB3 level of theory of the bond dissociation energies for the butan-1-ol molecule have been reported. The predicted order of the C–H bond dissociation energies, which is significant for H-abstraction rates in particular, is as follows:

$$\alpha < \gamma < \beta < \delta < \mathrm{OH}$$

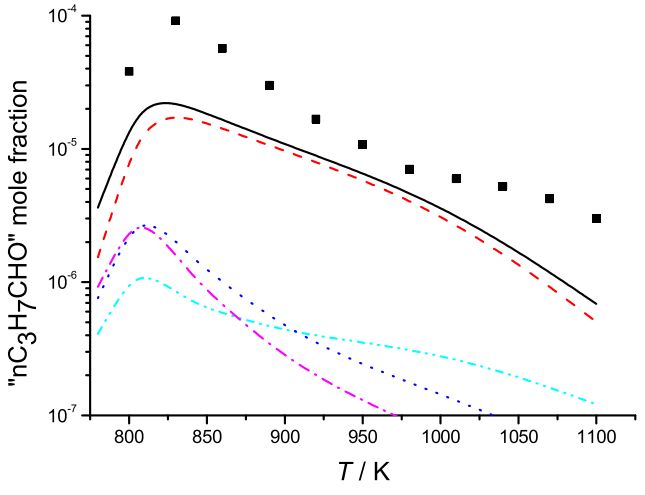

Fig. 9. Experimental and model-predicted profiles for butanal formation at 0.1% butan-1-ol, $\Phi = 2.0$, 10 atm, $\tau = 0.7$ s. ···· butanal, –·–· buten-3-ol, – – buten-2-ol, – – buten-1-ol, — total.

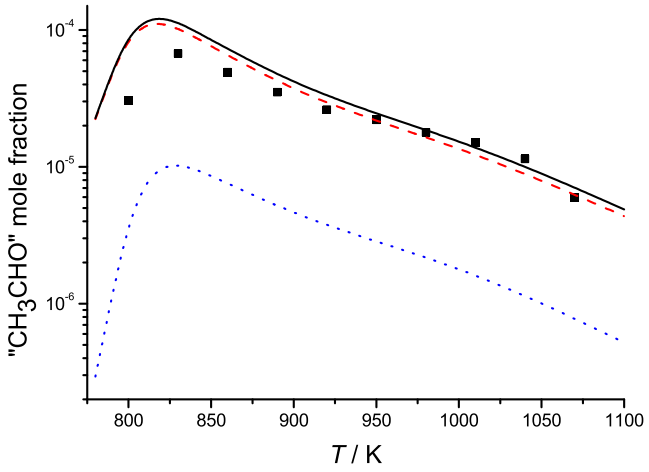

Fig. 10. Experimental and model-predicted profiles for acetaldehyde formation at 0.1% butan-1-ol, $\Phi = 0.5$, 10 atm, $\tau = 0.7$ s. ···· ethanal, – – ethenol, — total.

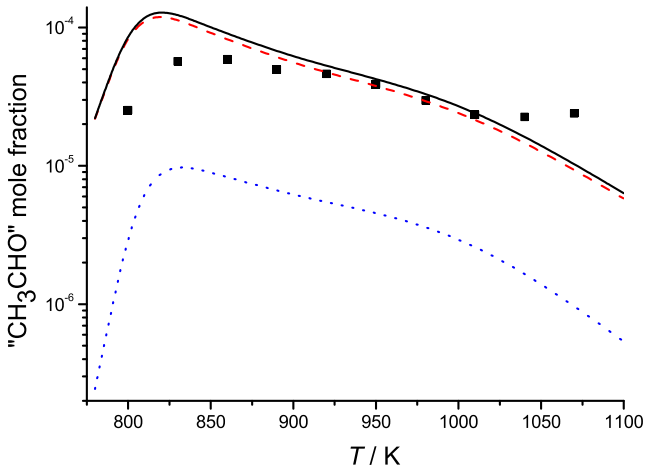

Fig. 11. Experimental and model-predicted profiles for acetaldehyde formation at 0.1% butan-1-ol, $\Phi = 1.0$, 10 atm, ··· ethanal, – – ethenol, — total.

Interestingly, the dissociation energy of the C_γ–H bond was found to be intermediate between that of the C_α–H and C_β–H. A comparison with equivalent results for ethanol and *n*-propanol indicates that both C_α–H and O–H bond energies are essentially independent of the length of the carbon chain for these straight chain alcohols.

Taking into account these computational results for butan-1-ol, a detailed chemical kinetic model has been constructed and used to simulate the above ignition delay data, with good agreement. Jet-stirred reactor species profiles [14] have also been simulated, resulting in reasonable agreement.

An attempt has been made at including enol chemistry in our models and it is shown that these species play a not insignificant role in the combustion chemistry of alcohols. Clearly, experimental verification with advanced analytical techniques is required to confirm these suppositions.

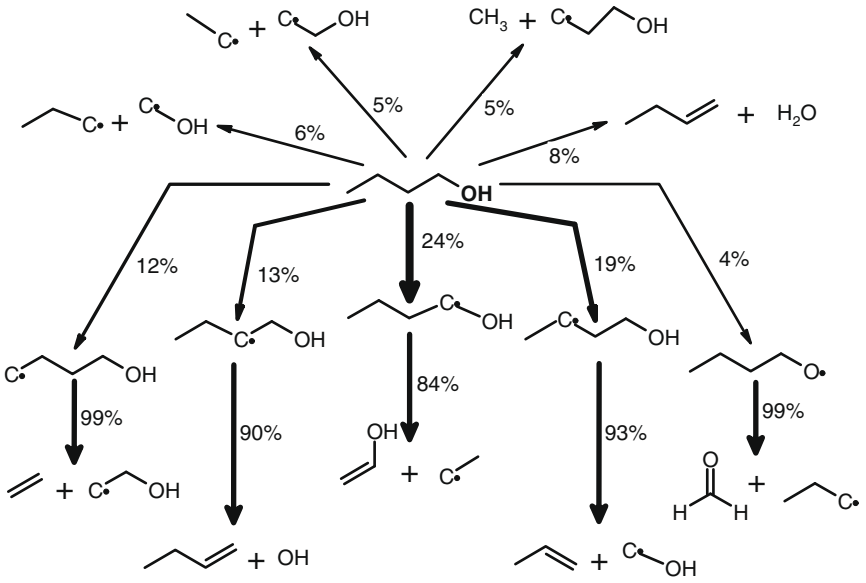

Fig. 12. Reaction path analysis for butan-1-ol in the shock tube; $\Phi = 1$, 1450 K, 1 atm, 20% consumption.

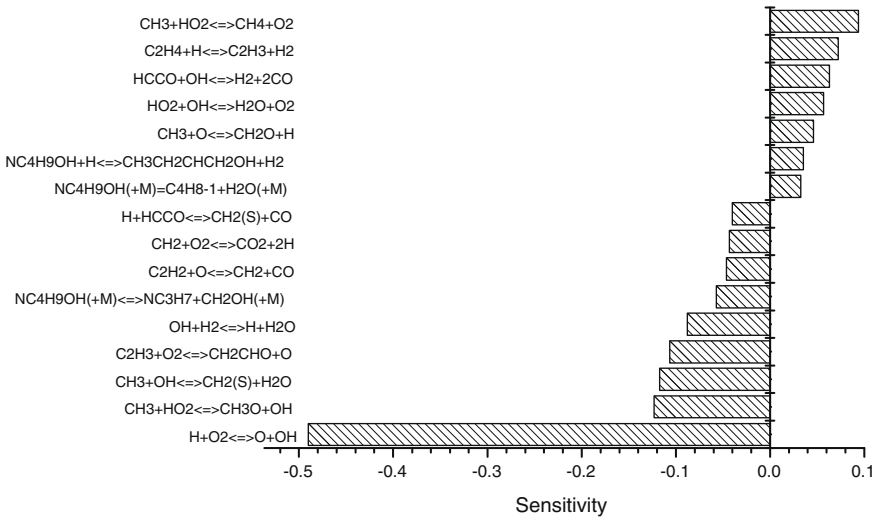

Fig. 13. Sensitivity study of ignition delay; 1450 K, $\Phi = 2$ and 1 atm.

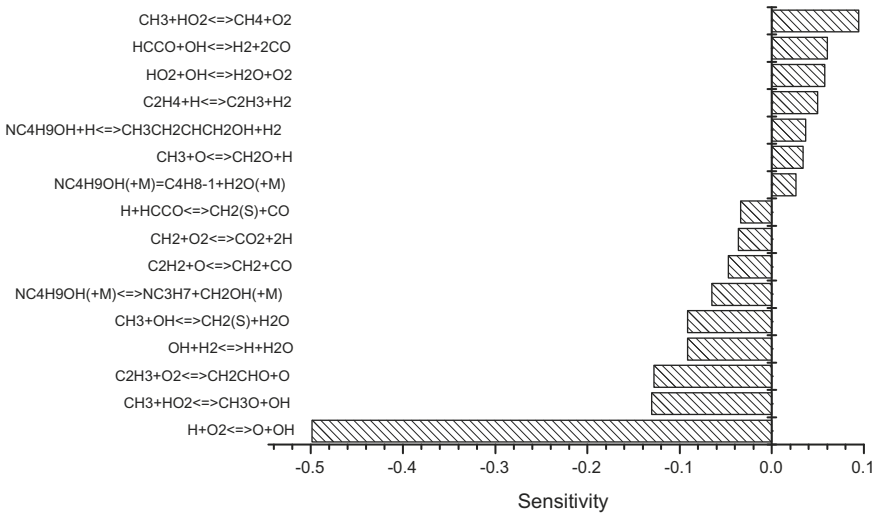

Fig. 14. Sensitivity study of ignition delay; 1450 K, $\Phi = 2$ and 2.6 atm.

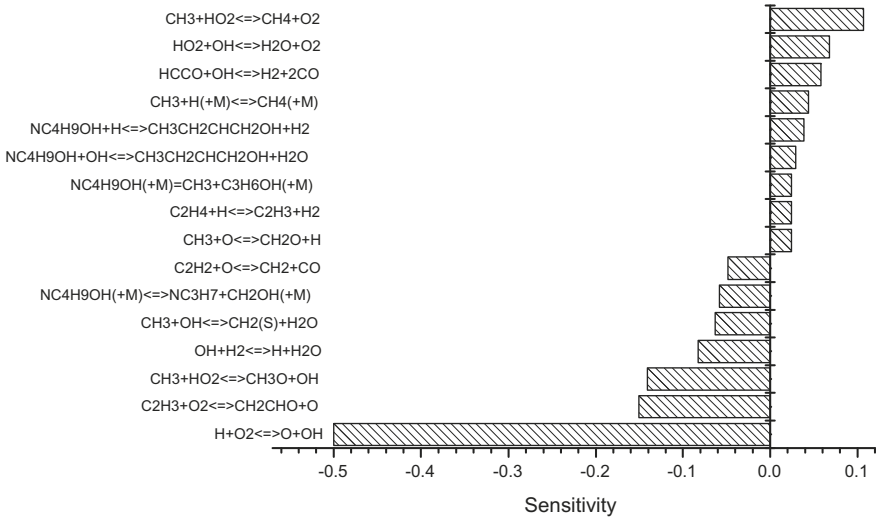

Fig. 15. Sensitivity study of ignition delay; 1450 K, $\Phi = 2$ and 8 atm.

Acknowledgments

GB thanks the Irish Research Council for Science, Engineering and Technology. SP and VZ hold EU Marie Curie Fellowships, ENK6-CT2002-50516. Funding from an EU Marie Curie Transfer of Knowledge Grant (MKTD-CT-2004-517248) is acknowledged and we thank the Irish Centre for High-End Computing, ICHEC, for provision of computational resources.

References

[1] J.S. Dukes, Climactic Change 61 (2003) 31–44.
[2] L.D. Gomez, C.G. Steele-King, S.J. McQueen-Mason, New Phytol. 178 (2008) 473–485.
[3] M.Z. Jacobson, Environ. Sci. Technol. 41 (2007) 4150–4157.
[4] D. Mackay, N. de Sieyes, M. Einarson, K. Feris, A. Pappas, I. Wood, L. Jacobsen, L. Justice, M. Noske, J. Wilson, C. Adair, K. Scow, Environ. Sci. Technol. 41 (2007) 2015–2021.
[5] T.C. Ezeji, N. Qureshi, H.P. Blaschek, Curr. Opin. Biotech. 18 (2007) 220–227.
[6] M. Golombok, S. Tierney, Ind. Eng. Chem. Res. 36 (1997) 5023–5027.
[7] T. Wallner, S.A. Miers, S. McConnell, in: Proc. Spring Tech. Conf. ASME Internal Combustion Engine Division Chicago, April 27–30, 2008, pp. 129–139.
[8] S. Atsumi, T. Hanai, J.C. Liao, Nature 451 (2008) 86–89.
[9] W.L. Luyben, Energ Fuel 22 (2008) 4249–4258.
[10] J.A. Barnard, T. Faraday Soc. 53 (1957) 1423–1430.
[11] C.S. McEnally, L.D. Pfefferle, Proc. Combust. Inst. 30 (2005) 1363–1370.
[12] B. Yang, P. Owald, Y. Li, J. Wang, L. Wei, Z. Tian, F. Qi, K. Kohse-Höinghaus, Combust. Flame 148 (2007) 198–209.
[13] P. Dagaut, C. Togbé, Fuel 87 (2008) 3313–3321.
[14] P. Dagaut, S.M. Sarathy, M.J. Thomson, Proc. Combust. Inst. 32 (2009) 229–237.
[15] S.M. Sarathy, M.J. Thomson, C. Togbé, P. Dagaut, F. Halter, C. Mounaim-Rousselle, Combust. Flame (2009) 852–864.
[16] J.T. Moss, A.M. Berkovitz, M.A. Oehlschlaeger, J. Biet, V. Warth, P. Glaude, F. Battin-Leclerc, J. Phys. Chem. A 112 (2008) 10843–10855.
[17] S. Dooley, H.J. Curran, J.M. Simmie, Combust. Flame 153 (2008) 2–32.
[18] W.K. Metcalfe, S. Dooley, H.J. Curran, J.M. Simmie, A.M. El-Nahas, M.V. Navarro, J. Phys. Chem. A 111 (2007) 4001–4014.
[19] A. Toland, J.M. Simmie, Combust. Flame 132 (2003) 556–564.
[20] C.A. Daly, J.M. Simmie, J. Würmel, N. Djebaili, C. Paillard, Combust. Flame 125 (2001) 1329–1340.
[21] C.A. Daly, J.M. Simmie, P. Dagaut, M. Cathonnet, Combust. Flame 125 (2001) 1106–1117.
[22] P. Dagaut, C. Daly, J.M. Simmie, M. Cathonnet, Proc. Combust. Inst. 27 (1998) 361–369.
[23] P. Dagaut, M. McGuinness, J.M. Simmie, M. Cathonnet, Combust. Sci. Technol. 135 (1998) 3–29.
[24] P. Dagaut, M. Cathonnet, M. McGuinness, J.M. Simmie, Combust. Flame 110 (1997) 409–417.
[25] P. Dagaut, M. McGuinness, J.M. Simmie, M. Cathonnet, Combust. Sci. Technol. 129 (1997) 1–16.
[26] J. Würmel, M. McGuinness, J.M. Simmie, J. Chem. Soc., Faraday Trans. 92 (1996) 715–721.

[27] P. Dagaut, D. Voisin, M. Cathonnet, M. McGuinness, J.M. Simmie, Combust. Flame 106 (1996) 62–68.
[28] P. Dagaut, M. Reuillon, D. Voisin, M. Cathonnet, M. McGuinness, J.M. Simmie, Combust. Sci. Technol. 107 (1995) 301–316.
[29] M.P. Dunphy, J.M. Simmie, Combust. Flame 85 (1991) 489–498.
[30] M.P. Dunphy, J.M. Simmie, Int. J. Chem. Kinet. 23 (1991) 553–558.
[31] M.P. Dunphy, P.M. Patterson, J.M. Simmie, J. Chem. Soc., Faraday Trans. 87 (1991) 2549–2559.
[32] M.P. Dunphy, J.M. Simmie, J. Chem. Soc., Faraday Trans. 87 (1991) 1691–1696.
[33] M.P. Dunphy, J.M. Simmie, Combust. Sci. Technol. 66 (1989) 157–161.
[34] J. Moc, J.M. Simmie, H.J. Curran, J. Mol. Struct. 928 (2009) 149–157.
[35] J. Moc, G. Black, J.M. Simmie, H.J. Curran, in: International Conference on Computational Methods in Science Engineering, Hersonissos, Greece, 2008.
[36] [36] J.M. Simmie, H.J. Curran, J. Phys. Chem. A 113 (2009) 7834–7845.
[37] C. Morley, Gaseq v0.76, <http://www.gaseq.co.uk>.
[38] E.R. Ritter, J.W. Bozzelli, Int. J. Chem. Kinet. 23 (1991) 767–778.
[39] S.W. Benson, Thermochemical Kinetics, John Wiley & Sons, New York, 1976.
[40] S.E. Stein, R.L. Brown, in: P.J. Linstrom, W.G. Mallard (Eds.), Structures and Properties Group Additivity Model in NIST Chemistry WebBook, NIST Standard Reference Database Number 69, June 2005, National Institute of Standards and Technology, Gaithersburg MD, 20899. <http://webbook.nist.gov>.
[41] A. Burcat, B. Ruscic, Ideal Gas Thermochemical Database with Updates from Active Thermochemical Tables <ftp://ftp.technion.ac.il/pub/supported/aetdd/thermodynamics>, 2008 (14.07.08).
[42] D.C. Horning, D.F. Davidson, R.K. Hanson, J. Propul. Power 18 (2002) 363–371.
[43] J.M. Smith, J.M. Simmie, H.J. Curran, Int. J. Chem. Kinet. 37 (2005) 728–736.
[44] Y-R. Luo, Comprehensive Handbook of Chemical Bond Energies, CRC Press, Boca Raton, 2007.
[45] J.A. Montgomery, M.J. Frisch, J.W. Ochterski, G.A. Petersson, J. Chem. Phys. 110 (1999) 2822–2827.
[46] J.A. Montgomery, M.J. Frisch, J.W. Ochterski, G.A. Petersson, J. Chem. Phys. 112 (2000) 6532–6542.
[47] Frisch, M.J. et al., Gaussian 03, Revision D.01, Gaussian, Inc., Wallingford CT USA, 2004.
[48] W.J. Hehre, R. Ditchfield, L. Radom, J.A. Pople, J. Am. Chem. Soc. 92 (1970) 4796–4801.
[49] A.M. El-Nahas, J.W. Bozzelli, J.M. Simmie, M.V. Navarro, G. Black, H.J. Curran, J. Phys. Chem. A 110 (2006) 13618–13623.
[50] K. Ohno, H. Yoshida, H. Watanabe, T. Fujita, H. Matsuura, J. Phys. Chem. 98 (1994) 6924–6930.
[51] H.A. Gundry, D. Harrop, A.J. Head, G.B. Lewis, J. Chem. Thermodyn. 1 (1969) 321–332.
[52] J.H.S. Green, Chem. Ind. (London) (1960) 1215–1216.
[53] H.A. Skinner, A. Snelson, T. Faraday Soc. 56 (1960) 1776–1783.
[54] A.I. Sachek, A.D. Peshchenko, D.N. Andreevskii, Vestsi Akad. Navuk BSSR, Ser. Khim. Navuk 1 (1978) 124–126.
[55] J.B. Pedley, R.D. Naylor, S.P. Kirby, Thermochemical Data of Organic Compounds, second ed., Chapman Hall, New York, 1986.
[56] B. Ruscic, J. Berkowitz, J. Chem. Phys. 101 (1994) 10936–10946.
[57] J.L. Holmes, Int. J. Mass Spectrom. 118/119 (1992) 381–394.
[58] J.W. Ochterski, G.A. Petersson, J.A. Montgomery Jr., J. Chem. Phys. 104 (1996) 2598–2619.
[59] M. Yujing, A. Mellouki, Chem. Phys. Lett. 333 (2001) 63–68.
[60] F. Cavalli, H. Geiger, I. Barnes, K.H. Becker, Environ. Sci. Technol. 36 (2002) 1263–1270.
[61] A. Galano, J.R. Alvarez-Idaboy, G. Bravo-Pérez, M.E. Ruiz-Santoyo, Phys. Chem. Chem. Phys. 4 (2002) 4648–4662.
[62] B. Ruscic, J.E. Boggs, A. Burcat, A.G. Csaszar, J. Demaison, R. Janoschek, J.M.L. Martin, M.L. Morton, M.J. Rossi, J.F. Stanton, P.G. Szalay, P.R. Westmoreland, F. Zabel, T. Berces, J. Phys. Chem. Ref. Data 34 (2005) 573–656.
[63] V.E. Tumanov, E.T. Denisov, Kinet. Catal. 45 (2004) 621–627.
[64] W. Tsang, in: Energetics of Stable Molecules and Reactive Intermediates, NATO Science Series C 535, 1999, pp. 323–352.
[65] H. Sun, J.W. Bozzelli, J. Phys. Chem. A 105 (2001) 4504–4516.
[66] V.V. Takhistov, Organic Mass Spectrometry, Nauka, Leningrad, 1990.
[67] D. Fulle, H.F. Hamann, H. Hippler, C.P. Jansch, Phys. Chem. Chem. Phys. 101 (1997) 1433–1442.
[68] S.W. Benson, H.E. O'Neal, Free Radicals, vol. II, Wiley, New York, 1973.
[69] L. Batt, K. Christie, R.T. Milne, A.J. Summers, Int. J. Chem. Kinet. 6 (1974) 877–885.
[70] E.T. Denisov, E.G. Denisova, Handbook of Antioxidants, CRC Press, New York, 2000.
[71] A. Hatipoğlu, Z. Çinar, J. Mol. Struct. Theochem 631 (2003) 189–207.
[72] G. Bourque, D. Healy, H.J. Curran, C. Zinner, D. Kalitan, J. de Vries, C. Aul, E. Petersen, Proc. ASME Turbo Expo. 3 (2008) 1051–1066.
[73] F. Battin-Leclerc, R. Fournet, P.A. Glaude, B. Judenherc, V. Warth, G.M. Côme, G. Scacchi, Proc. Combust. Inst. 28 (2000) 1597–1605.
[74] W. Tsang, J. Phys. Chem. Ref. Data 19 (1990) 1–68.
[75] W. Tsang, J. Phys. Chem. Ref. Data 17 (1988) 887–952.
[76] A.M. Dean, J. Phys. Chem. 89 (1985) 4600–4608.
[77] A.M. Dean, J.M. Bozzelli, E.R. Ritter, Combust. Sci. Tech. 80 (1991) 63–85.
[78] R.G. Gilbert, K. Luther, J. Troe, Ber. Bunsenges. Phys. Chem. 87 (1983) 169–177.
[79] W. Tsang, Int. J. Chem. Kinet. 8 (1976) 173–192.
[80] J.P. Orme, H.J. Curran, J.M. Simmie, J. Phys. Chem. A 110 (2006) 114–131.
[81] J. Park, Z.F. Xu, M.C. Lin, J. Chem. Phys. 118 (2003) 9990–9996.
[82] Z.F. Xu, J. Park, M.C. Lin, J. Chem. Phys. 120 (2004) 6593–6599.
[83] C.W. Wu, Y.P. Lee, S. Xu, M.C. Lin, J. Phys. Chem. A 111 (2007) 6693–6703.
[84] Unpublished calculations at CBS-QB3 and CBS-APNO levels of theory.
[85] H.J. Curran, Int. J. Chem. Kinet. 38 (2006) 250–275.
[86] C.A. Taatjes, N. Hansen, A. McIlroy, J.A. Miller, J.P. Senosiain, F. Qi, L. Sheng, Y. Zhang, T.A. Cool, J. Wang, P.R. Westmoreland, M.E. Law, T. Kasper, K. Kohse-Höinghaus, Science 308 (2005) 1887–1889.
[87] Chemkin-Pro™, Reaction Design Inc., San Diego, Calif.
[88] W.K. Metcalfe, C. Togbé, P. Dagaut, H.J. Curran, J.M. Simmie, Combust. Flame 156 (2009) 250–260.